FAST CURRENT MAPPING OF PHOTOVOLTAIC DEVICES USING COMPRESSIVE SAMPLING

George Koutsourakis[a]*, Xiaofeng Wu[a], Matt Cashmore[b], Simon Hall[b], Martin Bliss[a], Thomas R. Betts[a], Ralph Gottschalg[a]
[a] Centre for Renewable Energy Systems Technology (CREST), School of Electronic, Electrical and Systems Engineering, Loughborough University, Loughborough, Leicestershire, LE11 3TU, UK
[b] National Physics Laboratory (NPL), Hampton Road, Teddington, Middlesex, TW11 0LW, UK
*Tel.: +44 1509 635303, Email: G.Koutsourakis@lboro.ac.uk

ABSTRACT: Compressed sensing (CS) sampling theory is applied to the Light Beam Induced Current (LBIC) measurement technique in order to significantly reduce measurement time while maintaining or increasing accuracy. Using this method, a current map of the device can be reconstructed from far fewer measurements by means of an optimisation algorithm. Measurement simulations are implemented using a two dimensional photovoltaic (PV) device model to explore the capabilities and limitations of the method. A physical realisation of the technique is demonstrated. The raster scanning process of the LBIC system is replaced with a Digital Micro-mirror Device (DMD) pattern projection system. Measurement speed is also improved due to the response time of the DMD pattern generator, which is less than 20μs. An experimental CS-LBIC setup, alongside with initial experimental results that indicate the feasibility of the method are presented.
Keywords: Characterisation, Compressed Sensing, Simulation

1. INTRODUCTION

Characterisation of devices is key for advancement of photovoltaic (PV) technologies. The commercialisation of PV leads to larger devices which need to have uniform quality over their area. Thus PV device spatial characterisation is crucial for the development of this technology.

Well established techniques exist for spatial characterisation, such as Electroluminescence (EL) [1], Photoluminescence (PL) [2], Lock-In Thermography (LIT) [3] and Light Beam Induced Current (LBIC) measurements [4]. These methods are complementary to each other and each produce different kinds of information.

The spatial current response of PV cells is quantitatively measured using the LBIC method [4][5]. Measurements are implemented by applying a point by point scan with a collimated light source, producing a current map and delivering quantitative information about the electrical, optical and material properties of PV cells [6] or modules [7]. The spot on the sample that realises the scan usually has a size of several micrometres, which means that measurements are cumbersome and time-consuming. The time taken for the scan is really the main drawback of LBIC measurements and limits wider application of this technique.

To overcome this issue, the application of the Compressed Sensing (CS) sampling theory on LBIC measurements is considered in this work. According to this theory, one can reconstruct a signal using an incomplete measurement dataset [8][9]. For the realisation of CS-LBIC measurements, instead of a point by point scan, a series of pattern - test functions are projected on the sample. The current response is measured for each pattern. Fewer measurements than points of the final current map are taken and the image is reconstructed via optimisation algorithms. For the physical implementation of the measurement, the generation of the test patterns is achieved utilising a Digital Micromirror Device (DMD) [10]. The fast response of the DMD kit and the fewer measurements needed for acquiring the current map lead to the significant reduction of measurement time comparing to standard LBIC systems.

The limitations of this approach are demonstrated here based on simulations using spatially-resolved modelling techniques with the PV-Oriented Nodal Analysis (PVONA) tools developed in CREST [11]. Several different defects were simulated and compared with measurements of a prototype CS-LBIC experimental setup developed at the National Physics Laboratory (NPL).

2. BACKGROUND THEORY

2.1 Compressed sensing theory

As for all images, the image of the current map is compressible, which means it has a sparse representation using an appropriate basis. Images are usually compressed to be stored, for example as JPEG files. In this instance, the discrete cosine transform (DCT) is applied, after which the signal (image) can be described using a very small number of coefficients in the transform domain. In JPEG compression only the K larger coefficients are kept and the rest are put to zero. The aim of compressive sampling is to directly measure these K coefficients, acquiring M measurements, to reconstruct the N pixel image, where K<M<N. As the locations of the K coefficients in the transform domain are not known, M is larger than K but still, significantly smaller than N.

A compressed representation of a signal, **x**, is acquired using M<<N linear measurements between **x** and a set of test functions $\{\varphi_m\}_{m=1}^{M}$, forming $y[m]=\langle x,\varphi_m\rangle$ which is the actual measurement. The test functions $\{\varphi_m\}_{m=1}^{M}$ are represented as rows in a MxN matrix $\Phi=[\varphi_1,\varphi_2,\varphi_3,\ldots\varphi_m]$ and the problem can be written as:

$$\mathbf{y}=\Phi\mathbf{x} \qquad (1)$$

As a consequence of y having significantly fewer elements than x, there is loss of information. Since M<<N, there are infinitely many translations, $\{\mathbf{x}:\mathbf{y}=\Phi\mathbf{x}\}$. This is apparently an underdetermined problem with infinite solutions. However, a measurement matrix, Φ, can be designed such that an almost exact approximation of the signal **x** can be recovered from measurement **y**, if **x** is sparse or compressible. In practice, few real-world signals are truly sparse, although almost all of them are

compressible, meaning that they can be well-approximated by a sparse signal, or are sparse after a transform [12], which means their representation with a basis Ψ is sparse.

The signal reconstruction algorithm must take the M measurements in the vector **y**, the random measurement matrix Φ and the basis Ψ (transform); and reconstruct the N-length signal **x** or, equivalently, its sparse coefficient vector **α**, as **x**=Ψ**α** and **y**=Φ**x**=ΦΨ**α**. The solution to the underdetermined problem is the **x** vector (or more precisely the α vector) with the minimum ℓ_1 norm [13]:

$$\hat{\mathbf{x}}=\text{argmin}\|\mathbf{x}\|_1 \text{ subject to } \Phi\mathbf{x}=\mathbf{y} \qquad (2)$$

Or more precisely

$$\hat{\boldsymbol{\alpha}}=\text{argmin}\|\boldsymbol{\alpha}\|_1 \text{ subject to } \Phi\Psi\boldsymbol{\alpha}=\mathbf{y} \qquad (3)$$

This is a convex optimization problem that conveniently reduces to a linear program known as basis pursuit [9][14].

2.2 Application of compressed sensing on PV characterisation

Compressive sampling can be used as an alternative of standard LBIC measurements in order to reduce measurement time. Instead of a point by point scan a series of test functions $\{\varphi_m\}_{m=1}^{M}$ have to be projected on the PV device. Random binary matrices of ones and zeros can be used as patterns, as they are easy to implement and satisfy the requirements for compressive sampling [15]. For every projected pattern the current response of the PV device is measured, populating the measurement vector **y**, as illustrated in figure 1. Since the projected patterns are known, constructing sensing matrix Φ, the measured current map is reconstructed using equation (2) or (3). With this method, current maps can be acquired with much fewer measurements than what a raster scan would require.

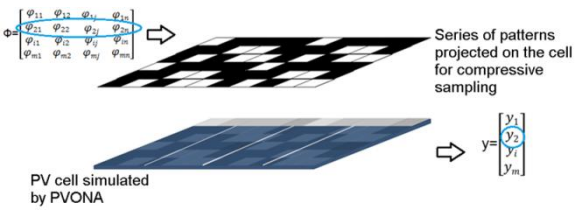

Figure 1: Diagram of the CS-LBIC measurement procedure. A series of random binary patterns is projected on the PV device, while the current response for every pattern is measured

2.3 PV Oriented Nodal Analysis (PVONA)

PVONA is a software toolset specifically developed for solving the spatially-resolved model (SRM) of PV devices. A PV cell can be described by a SRM in the form of a discrete nonlinear circuit network as shown in Figure 2(a). In the SRM, a PV cell is modelled by an array of sub-cells. Each local sub-cell corresponds to a finite rectangular-shaped area of the cell. The nonlinear behaviour of the local sub-cells (blocks with an arrow) is described by local diode models. The contact schemes are represented by two resistor networks.

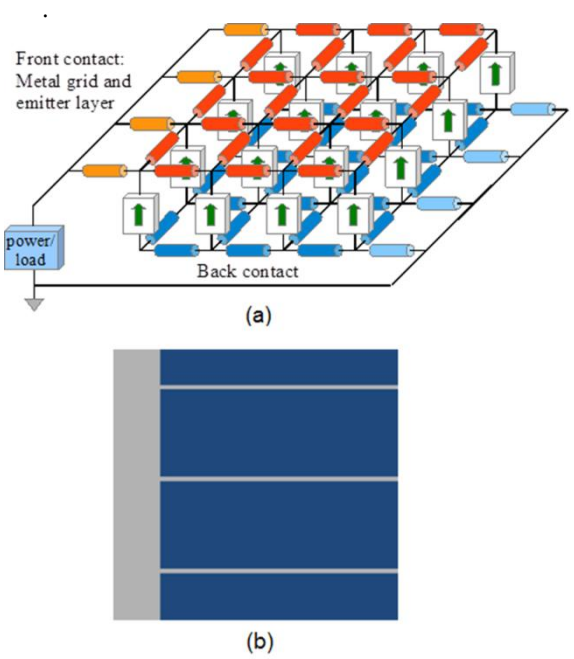

Figure 2: (a) Schematic of the structure of the SRM of a PV cell. (b) The layout of the front contact layer of the virtual c-Si sample used in this work.

The PVONA toolset can solve this type of SRMs efficiently by utilising an optimised parallel solver as described in [16]. It allows high-resolution (e.g. mega sub-cell) simulations of PV cells [11].

In this work, a virtual crystalline silicon (c-Si) cell (representing a reference cell) is configured for the simulation and study of CS-LBIC measurements. The layout of the front layer of the sample is illustrated in Figure 2(b). The sample consists of 60 × 60 sub-cells. A front contact layer is used to model the metal busbar and fingers. The busbar occupies 10 columns and each of the three fingers occupies one row. The resistance in the back contact in neglected. This assumption is valid for c-Si cells as discussed in [16]. The single-diode model is used to describe local electrical properties and the input parameters used are listed in Table 1. Defects can be introduced by changing local parameters. For example, a crack can be modelled by a series of sub-cells with reduced or zero photocurrent J_{ph} and a very high emitter resistance $R_{\blacksquare emitter}$ value, $R_{\blacksquare}$ being the sheet resistance.

Table 1 Input parameters of the SRM used in this work

J_{ph} (A/cm^2)	0.035
J_{sat} (A/cm^2)	5.0×10^{-7}
N	1.4
R_{sh} (Ω·cm^2)	8.35×10^{4}
R_s^i (Ω·cm^2)	0.05
$R_{\blacksquare emitter}$ (Ω/□)	80.0
$R_{\blacksquare grid}$ (Ω/□)	1.0×10^{-3}

The simulation of CS-LBIC experiments is done through the irradiance interface provided by the PVONA. For each operation, a binary matrix is used to represent the pattern projected on the sample. For an illuminated sub-cell,

the J_{ph} listed in Table 1 is applied. Otherwise the J_{ph} is set to zero for an inactive sub-cell. For each pattern, the short circuit current I_{SC} is recorded, populating measurement vector **y**, while each pattern is a row of sensing matrix Φ, thus the current map is reconstructed by equation (3). Random binary matrices are used as patterns and populate the sensing matrix, while the discrete cosine transform is applied (basis Ψ) to provide the sparse representation required. For the reconstruction the ℓ1 magic toolkit in MatLab is used, developed by Candès, Romberg and Tao [17].

3. SIMULATION RESULTS

For the implementation of the simulations a series of different cell configurations is used. In figure 3 the actual current maps of the different simulated samples are presented. Current is uniform in all active area of the cell and zero at the fingers and busbar. Apart from the sample with no defects, three of the configured samples with defects have lines of zero current, diagonal, vertical or parallel to the fingers, representing crack of different orientations. One sample has a dead spot and the last one a combination of a dead spot and a crack combining three possible orientations of lines. In this last case the current of the simulated crack was set to 50% of the current value of the active area, to provide a more realistic result. Except from the current, a high value of series resistance were also set in these defected areas in the SRM. The purpose of the different configurations is to investigate the performance of CS-LBIC measurements in detecting different types and orientations of defects. The different types of configured samples are presented in figure 2.

To evaluate the performance of CS-LBIC measurements a comparison has to be made between the current maps produced by the simulated CS-LBIC measurements and the real known current maps. For this purpose Normalised Root Mean Square Error (NRMSE) and the correlation coefficient ρ (Pearson's correlation coefficient) are calculated to compare images. NRMSE is calculated using:

$$\mathrm{NRMSE} = \frac{1}{x_{max}-x_{min}} \cdot \sqrt{\frac{\sum_{i=1}^{N} (\hat{x}_i - x_i)^2}{N}} \qquad (4)$$

Where noted with x_i are the elements of the real current map, $\hat{x}_i$ the pixel measurements by CS-LBIC measurements, N the number of pixels, which in our case are 3600 (60 x 60 current maps) and x_{max} and x_{min} the maximum and minimum values of the real current map. The correlation coefficient is calculated by dividing the covariance of the real and measured current map by the product of their standard deviations:

$$\rho(\hat{\mathbf{x}},\mathbf{x}) = \frac{\mathrm{cov}(\hat{\mathbf{x}},\mathbf{x})}{\sigma_{\hat{\mathbf{x}}} \cdot \sigma_{\mathbf{x}}} \qquad (5)$$

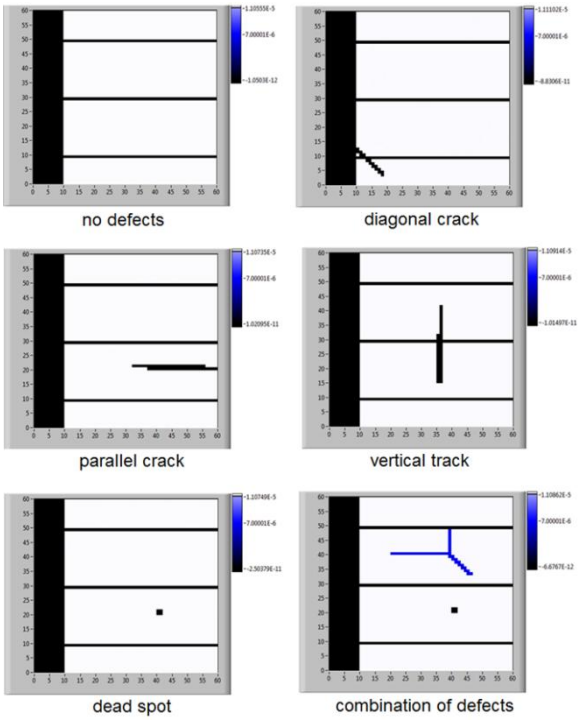

Figure 3: The different configurations of simulated samples with the SRM, for implementation of CS-LBIC simulations.60 x 60 pixel current maps were implemented for each case.

The number of measurements acquired every time with the CS-LBIC method is expressed as a percent of the number of pixels N. In the given case, a point by point scan would need N=3600 measurements to deliver the current map. CS-LBIC allows reconstructing a current map with fewer measurements. A 30% current map means that it has been produced by 1080 measurements. The improvement of the reconstruction by acquiring more measurements is clear as visible from figure 4.

In figure 5 the NRMSE and correlation graphs are presented as a function of number of acquired measurements. It is clear that all configured samples have the same behaviour; hence the technique performs in the same way for all types of features in PV devices. Above 30% of measurements correlation coefficient is more than 0.95 and as presented in figure 3, all features of the cell are visible, while the reconstruction NRMSE error is just above 10%. Above 40% of measurements the NRMSE becomes less than 10% for all samples and adding more measurements just makes the image clearer. It has to be noted that the real current map in this simulation is an extreme, unrealistic case where the current has the exact same value in all non-defect areas and the transition from active areas to non-active or defected areas is sharp, with no intermediate points. Moreover, standard LBIC measurements results would still not be identical to the current map as it would be affected by measurement noise.

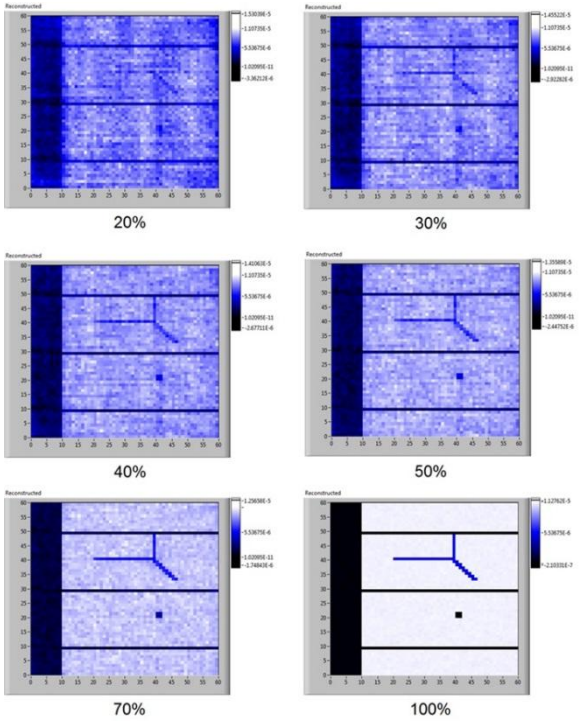

Figure 4: CS-LBIC simulation results of the 60x60 pixel current map, with increasing number of measurements.

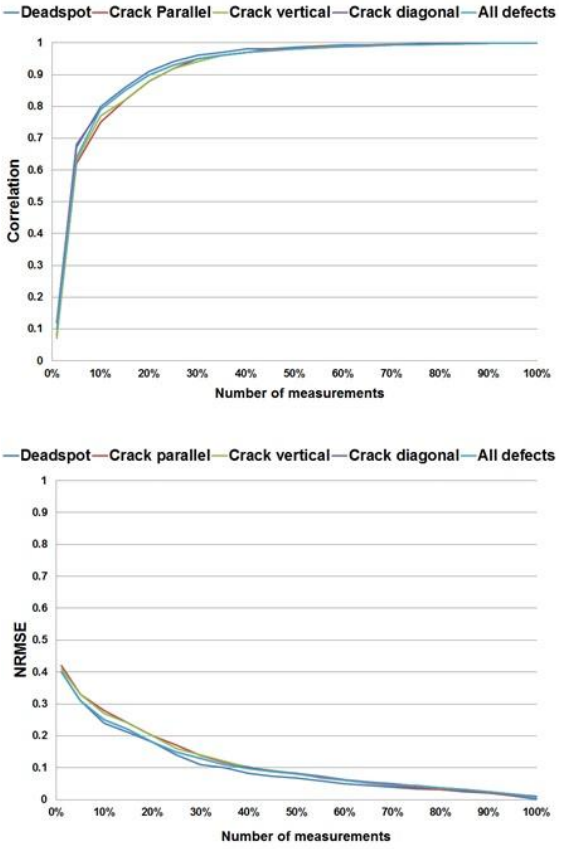

Figure 5: Correlation coefficient and NRMSE for all configured samples, as a function of number of measurements with the CS-LBIC method, compared with the real current map.

4. EXPERIMENTAL RESULTS WITH PROTOTYPE SYSTEM IN NPL

An initial prototype has been built in NPL, in order to test the feasibility of CS characterization of PV devices. The light sources available are a 40mW 658nm laser and a 100mW 785nm one. A single mode optical fiber delivers the light to the optical system. The beam is expanded and collimated before the DMD generates the series of patterns to be projected on the sample under measurement. The DMD array has a 1024x768 resolution, with each micromirror having a size of 13.7μm x 13.7μm, thus the DMD area is approximately 1.4cm by 1cm. A 768 x 768 area of the DMD is used to create square patterns and as a result the projection has a size of 1cm x 1cm. A double two lens system and a mirror are used to deliver the projection on the sample under test. A schematic diagram of the prototype setup is presented in figure 6.

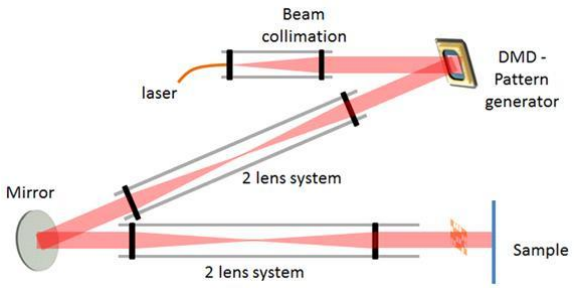

Figure 6: schematic diagram of the CS LBIC prototype in NPL.

An EFG (Edge-Defined, Film-Fed Growth) mc-Si encapsulated cell is used to test the experimental setup. An EL image of the sample is presented in figure 7, along with a 1cm by 1cm area selected for the measurements presented in this work. This small area includes similar features with the simulated samples, in order to compare the initial CS-LBIC measurements results with the simulations.

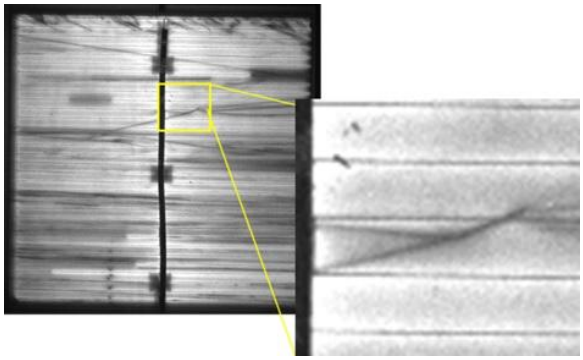

Figure 7: EL image of the mc-Si sample used for measurements and the 1cm x 1cm area for which results are presented in this work.

In figure 8 96x96 pixel current maps produced with the 785nm laser are presented. Each current map is produced applying different number of measurements, which is expressed as a percentage of the total number of pixels (9216). For instance the 30% current map is acquired by applying 2765 measurements, thus, having projected 2765 patterns on the sample. The improvement of the quality of

the current map when adding more measurements has a similar behaviour as in the case of the simulations, an indication that the physical implementation of the method used in the simulations is successful. However, there is a significant difference above 90% of measurements. Experimental results suggest worst measurement results when approaching 100% of measurements, which is what a raster scan would need. Reconstruction from 9216 measurements fails completely. The reason for this is the significant amount of noise present in the measurement system. No lock-in technique is used as the signal to noise ratio is high enough for the implementation of the measurements, although these noise levels are very high for a realisation of a raster scan. With fewer measurements available, the optimisation algorithm is less influenced by the noise levels, although when approaching 100% this issue becomes important. As simulations have no noise, the reconstruction from 100% of measurements is possible in that case.

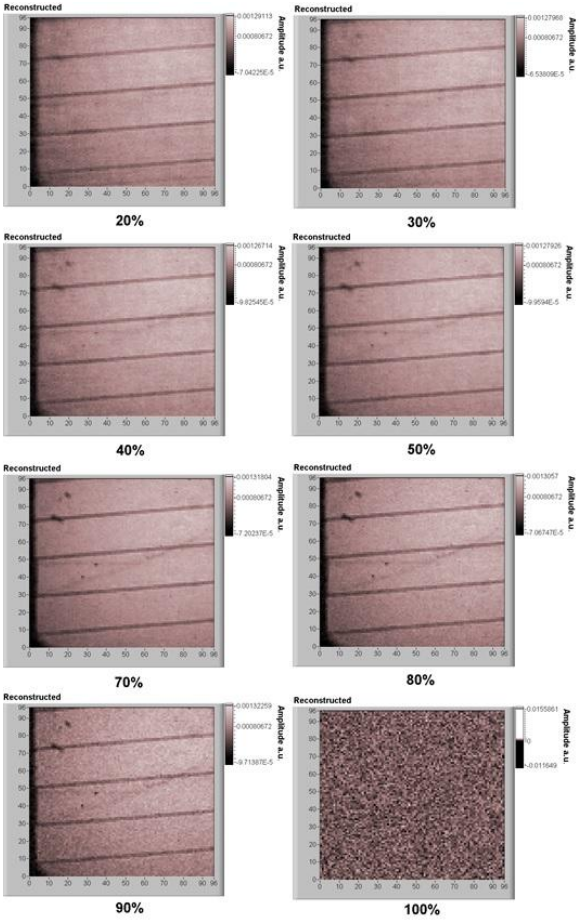

Figure 8 CS-LBIC measurement results of a 1cm x 1cm area of the mc-Si sample. Number of measurements acquired are expressed as a ratio of measurements by the total number of pixels.

All features present in the EL image are visible in the reconstructed images from 30% of measurements and above. Adding more measurements above 40% has no significant improvement, although it makes the image slightly clearer. The 785 wavelength laser has a penetration depth of only several micrometres from the surface of the sample, so the crack does not appear very bold like in the EL image, as it is probably mainly located in the bulk of the cell. The two spots on the top left of the maps seem to be surface effects so they have the same appearance in both EL and CS-LBIC images. Measurement results indicate that current maps of PV devices can be produced by acquiring much fewer measurements than with a standard LBIC system.

There is some distortion in the images due to a misalignment of the final projection on the sample, which is the reason for the skewed angles of fingers and bus-bars. Furthermore, irradiance is not perfectly uniform. This configuration is sufficient to demonstrate the feasibility of the proposed method but should be improved in the future.

5. CONCLUSIONS

A method for current mapping of PV devices is presented in this paper. The method is based on the compressed sensing sampling theory and can significantly reduce the measurement time of LBIC measurements for PV device characterization. Simulations of CS-LBIC measurements have been realised using the PVONA tools. The results show that this technique has the same performance for all types of features in samples.

A prototype experimental setup, built at NPL, is demonstrated. Measurement results show similar behaviour with the simulations and confirm the method's applicability for fast current mapping of PV devices. Although the cell area measured in this work is only 1cm by 1cm, the projection can be magnified in a straightforward way to scan larger areas, or even cells, in order to acquire current maps with the same methodology. On the other hand, the current setup is ideal for measurements of very small area devices usually produced in the research field of thin film solar cells and other emerging technologies such as organic or perovskite solar cells.

6. ACKNOWLEDGEMENTS

This work was funded through the European Metrology Research Programme (EMRP) Project ENG55 PhotoClass, which is jointly funded by the EMRP participating countries within EURAMET and the European Union. This work is co-funded by the UK National Measurement System and by the joint project 'Stability and Performance of Photovoltaics (STAPP)' funded by Research Councils UK (RCUK) Energy Programme in UK and by Department of Science and Technology in India.

7. REFERENCES

[1] T. Fuyuki and H. Kondo, "Photographic surveying of minority carrier diffusion length in polycrystalline silicon solar cells by electroluminescence," *Appl. Phys. Lett.*, vol. 86, no. 26, p. 262108, 2005.

[2] T. Trupke and R. Bardos, "Photoluminescence imaging of silicon wafers," *Appl. Phys. Lett.*, vol. 89, no. 4, p. 044107, 2006.

[3] O. Breitenstein, J. P. Rakotoniaina, and M. H. Al Rifai, "Quantitative evaluation of shunts in solar cells by

lock-in thermography," *Prog. Photovoltaics Res. Appl.*, vol. 11, no. 8, pp. 515–526, Dec. 2003.

[4] B. Sopori and A. Baghdadi, "Some investigations on the influence of defects/grain boundaries on photovoltaic mechanisms in polycrystalline silicon films," *Sol. Cells*, vol. 1, pp. 237–250, 1980.

[5] M. Stemmer, "Mapping of the local minority carrier diffusion length in silicon wafers," *Appl. Surf. Sci.*, vol. 63, pp. 213–217, 1993.

[6] J. Carstensen, G. Popkirov, J. Bahr, and H. Föll, "CELLO: an advanced LBIC measurement technique for solar cell local characterization," *Sol. Energy Mater. Sol. Cells*, vol. 76, no. 4, pp. 599–611, Apr. 2003.

[7] P. Vorasayan, T. R. Betts, and R. Gottschalg, "Limited laser beam induced current measurements: a tool for analysing integrated photovoltaic modules," *Meas. Sci. Technol.*, vol. 22, no. 8, p. 085702, Aug. 2011.

[8] E. Candes, J. Romberg, and T. Tao, "Stable signal recovery from incomplete and inaccurate measurements," *Comm. Pure Appl. Math.*, vol. 59, pp. 1207–1223, 2006.

[9] D. Donoho, "Compressed sensing," *Inf. Theory, IEEE Trans.*, vol. 52, no. 4, pp. 1289–1306, 2006.

[10] L. Hornbeck, "The DMDTM projection display chip: a MEMS-based technology," *Mrs Bull.*, vol. 26, no. 4, pp. 325–327, 2001.

[11] X. Wu, M. Bliss, A. Sinha, T. Betts, R. Gupta, and R. Gottschalg, "Distributed electrical network modelling approach for spatially resolved characterisation of photovoltaic modules," *IET Renew. Power Gener.*, vol. 8, no. 5, pp. 459–466, Jul. 2014.

[12] Y. Eldar and G. Kutyniok, *Compressed sensing: theory and applications*. Cambridge: Cambridge University Press, 2012.

[13] R. Baraniuk, "Compressive sensing," *IEEE Signal Process. Mag.*, vol. 24, no. July, pp. 1–9, 2007.

[14] E. Candès and M. Wakin, "An introduction to compressive sampling," *Signal Process. Mag. IEEE*, no. March 2008, pp. 21–30, 2008.

[15] R. Baraniuk, M. Davenport, R. DeVore, and M. Wakin, "A Simple Proof of the Restricted Isometry Property for Random Matrices," *Constr. Approx.*, vol. 28, no. 3, pp. 253–263, Jan. 2008.

[16] X. Wu, M. Bliss, A. Sinha, T. Betts, R. Gupta, and R. Gottschalg, "Accelerated Spatially Resolved Electrical Simulation of Photovoltaic Devices Using Photovoltaic-Oriented Nodal Analysis," *IEEE Trans. Electron Devices*, vol. 62, no. 5, pp. 1390–1398, 2015.

[17] E. Candès, J. Romberg, and T. Tao, "Robust uncertainty principles: Exact signal reconstruction from highly incomplete frequency information," *IEEE Trans. Inf. Therory*, vol. 52, no. 2, pp. 489–509, 2006.